GGPP depletion initiates metaflammation through disequilibrating CYB5R3-dependent eicosanoid metabolism

Lisha Wei[1,a], Yan-Yan Zheng[1,a], Jie Sun[1], Pei Wang[1], Tao Tao[1], Yeqiong Li[1], Xin Chen[1], Yongjuan Sang[1], Danyang Chong[1], Wei Zhao[1], Yuwei Zhou[1], Ye Wang[1], Zhihui Jiang[1], Tiantian Qiu[1], Chao-Jun Li[1,b], Min-Sheng Zhu[1,b], Xuena Zhang[1,b]

[1]State Key Laboratory of Pharmaceutical Biotechnology, Model Animal Research Center & Medical School of Nanjing University & Nanjing Drum Tower Hospital Affiliated by Nanjing University Medical School, Nanjing University, Nanjing 210061, China.

Running title: MVA pathway triggers metaflammation

[a] These authors contribute this work equally

[b] To whom correspondence should be addressed. Chao-Jun Li, The Model Animal Research Center, Nanjing University, Nanjing 210061, China. E-mail: licj@nju.edu.cn. Or Min-Sheng Zhu, The Model Animal Research Center, Nanjing University, Nanjing 210061, China. E-mail: zhums@nju.edu.cn; Phone: +86-25-58641529. Or Zhang Xue-Na, The Model Animal Research Center, Nanjing University, Nanjing 210061, China. E-mail: zhangxn@nicemice.cn; Phone: +86-25-58641526

ABSTRACT

Metaflammation is a primary inflammatory complication of metabolic disorders characterized by altered production of many inflammatory cytokines, adipokines and lipid mediators. While multiple inflammation networks have been identified, the mechanisms by which metaflammation is initiated have long been controversial. As mevalonate pathway (MVA) produces abundant bioactive isoprenoids and abnormal MVA has a phenotypic association with inflammation/immunity, we speculate that isoprenoids from the MVA may provide a causal link between metaflammation and metabolic disorders. Using a line with the MVA isoprenoids producer geranygeranyldiphosphate synthase (GGPPS) deleted, we find that GGPP depletion causes an apparent metaflammation as evidenced by abnormal accumulation of fatty acids, eicosanoid intermediates and proinflammatory cytokines. We also find that GGPP prenylate cytochrome b5 reductase 3 (CYB5R3) and the prenylated CYB5R3 then translocate from the mitochondrial to ER pool. As CYB5R3 is a critical NADH-dependent reductase necessary for eicosanoids metabolism in ER, we thus suggests that GGPP-mediated CYB5R3 prenylation is necessary for eicosanoid metabolism. In addition, we observe that pharmacological inhibition of MVA pathway by simvastatin is sufficient to inhibit CYB5R3 translocation and induces smooth muscle death. Therefore, we conclude that the dysregulation of MVA intermediates is an essential mechanism for metaflammation initiation, in which the imbalanced production of eicosanoid intermediates in ER serve as an important pathogenic factor. Moreover, the interplay of MVA and eicosanoids metabolism as we reported here illustrates a model for the coordinating regulation among metabolite pathways.

INTRODUCTION

In obesity and several metabolic disorders, altered production of many inflammatory cytokines, adipokines, lipid mediators and signalling through a plethora of immune receptors and intracellular mediators have been complicated. Such a metabolically triggered inflammation is called metaflammation (1), and now it is usually represents a state of chronic low-grade inflammation as a response to metabolic or nutrients disruption from one or more sources. It has been well demonstrated that metaflammation impacts seriously on

the progression of the diseases (2). Current knowledge shows that the integration of metabolic and inflammatory signalling network occurs at multiple levels, but how the metabolic disorders start with inflammation have long been unclear. In light of the phenotypic association of MVA pathway with inflammation/immunity (3), we hypothesized that MVA pathway might be a metabolic pathway triggering metaflammation.

The MVA pathway is fundamental for cholesterol biosynthesis and acts as an essential therapeutic target of lowing lipid (4). This pathway begins with synthesis of 3-hydroxy-3-methylglutaryl-Coenzyme A (HMG-CoA) by HMG-CoA synthase and then conversion of the resultant HMG-CoA to mevalonic acid by HMG-CoA reductase (HMGCR), the rate-limiting enzyme of MVA pathway. By over 20 subsequent enzyme reactions along this pathway, cholesterol is synthesized by post-squalene pathway, and meanwhile several bioactive intermediaries and end-products are produced by a non-sterol pathway. These non-sterol metabolites include isoprenoids, dolichol, ubiquinone and isopentenyladenine. Among these metabolites, farnesyl diphosphate (FPP) and GGPP are the primary forms of isoprenoids capable of modifying proteins (5). Protein prenylation is a class of lipid modification of proteins, in which the FPP (15-carbon) or GGPP (20-carbon) isoprenoids are covalently added to a conserved cysteine residues (e.g. CAAX and CCXX) at or near the C-terminus of proteins. This modification enables the proteins to interact with membrane or other proteins (5), but usually does not affect protein stability and activity (6). There are reports showing that small GTPases including RAS, RHO and RAB may be prenylated and translocated to membrane (7,8)

GGPP is produced by GGPPS with sequential condensation reactions of dimethylallyl-diphosphate with three units of isopentenyl-diphosphate (IPP), and geranygeranylate proteins by geranylgeranyltransferase I /II (GGTase I/II). As such a prenylation process is attenuated by MVA inhibition (9), MVA pathway seems to be required for the protein prenylation. More than 100 proteins with prenylation motif of GGPP have been identified so far (10), and the prenylated proteins participate multiple processes including tumorigenesis (11,12), glucose metabolism (13,14), apoptosis (15) and adipocyte browning (16). Based on

clinical observations from the mevalonate kinase deficiency (MKD) patients with mevalonate kinase loss-of function gene mutation, however, the syndromes caused by the impairment of MVA pathway are primarily exhibited by auto-inflammation and auto-immune disorders (3). We thus speculated that MVA pathway served as an important regulator of sterile inflammation. This point is also supported by recent observations (17,18).

HMGCR inhibitors such as statins are widely-used as lipid-lowing drugs by down-regulating cholesterol synthesis (9). Several reports show that administration of these drugs preferentially impairs vascular smooth muscle and blood pressure (19-25). The vascular smooth muscle seems sensitive to the impairment of MVA pathway. In addition, there are accumulating evidence showing a close relation of vascular smooth muscle in metabolic inflammation (26) (27). We thus examined the role of GGPPS in vascular smooth muscle cells. By analyzing a mouse line with smooth muscle-specific deletion of *Ggps1*, we surprisingly found that the mutant mice displayed abnormal expression of the genes related to inflammation and immunity, along with a progressive apoptosis of VSMCs. The addition of exogenous GGPP was able to restore the apoptosis process *in vitro*. Moreover, the deletion of GGPPS resulted in a significant increase in polyunsaturated fatty acids (PUFAs), showing an impaired eicosanoid production. This effect was attributable to abolished prenylation of CYB5R3 and hence failed translocation from mitochondria to ER pool. As CYB5R3 was a required reductase for maintaining microsomal oxidation/reduction environment necessary for eicosanoid metabolism, we concluded that GGPP produced by MVA pathway essentially regulated eicosanoids homeostasis. As the eicosanoids are closely related to inflammation and immunity, our result reveals a link of MVA or cholesterol biosynthesis with metaflammation.

RESULTS
MVA metabolism and GGPPS expression in postnatal aorta smooth muscle
In postnatal animals, to adapt new environments, milk nutrition and developmental requirements, such tissues as blood vessel remodel their metabolic programs. Among these programmes, cholesterol biosynthesis is particularly

2

important for synthesis of membrane material necessary for cell proliferation. We firstly measured MVA-associated genes in developing aorta smooth muscle tissues by a real-time PCR assay. From E18.5 to adult, *Ggps1*, farnesyl diphosphate synthase (*Fdps*) and *Hmgcr* genes were expressed in relatively constant level. The maximum difference was within 4-fold (Fig. 1*A*), showing the important role of MVA metabolism during aorta smooth muscle development. The expression of *Ggps1* was especially stable until d25. We also measured the genes related to glycolysis (*Hk2, Pfkp, Ldhb* and *Pdk2*), lipolysis (*Lpl*), β-oxidation (*Cpt1a* and *Acadl*), lipogenesis (*Fasn*) and mitochondrial oxidation (*Cox4i1, Cox7a1*). The expression levels of glucose and lipid metabolism-associated genes showed significant change with development and each played an important role at different stages (Fig. 1, *B-D*).

Expression of GGPPS in smooth muscle is required for the survival of neonatal mice

To determine the role of GGPP/GGPPS *in vivo*, we established a line with smooth muscle-specific deletion of *Ggps1* gene by crossing *Ggps1flox/flox* mice with SMA-Cre mice. The resultant *Ggps1flox/flox; SMA-Cre+* (*Ggps1SMKO*) mice were used as knockout (KO) mice and *Ggps1flox/flox;* SMA-Cre- or *Ggps1flox/+*; SMA-Cre- mice were used as control (CTR) mice (Fig. 2*A*). Western blot assay showed that KO aorta expressed GGPPS less than 10% of CTR, and KO jejunum smooth muscle expressed 40% (Fig. 2, *B* and *C*). The birth of KO and CTR pups obeyed Mendelian ratio, but the KO pups started to die from 5 weeks after birth (Fig. 2*E*). The body weights of KO mice at 6 weeks were slightly reduced (CTR: 21.71±2.78 g *vs* KO: 18.47±3.18 g, p<0.05) (Fig. 2*D*). Macro phenotypic examination for the mutant mice showed normal morphologies of the main organs including brain, lung, gut, bladder, airway, liver and skeletal muscle (Fig. S1, *A-C* and *F-J*). The mutant hearts appeared slightly larger, but their histology and function show no apparent alteration (Fig. S1*E* and Table S1). To our surprise, the systolic blood pressure (SBP) of the KO mice at 7-week old was significantly reduced (from 116±6.61 mmHg of CTR to 66±11.86 mmHg; p<0.0001) (Fig. 2*F*). Such a low SBP might cause severe cardiovascular disease and death (28,29). In addition, no aorta aneurysms phenotype was observed in

the mutant mice (Fig. S1*D*). Thus, our observation indicates that that the hypotension induced by GGPPS deletion may be the leading cause of animal death.

GGPPS deletion impairs artery smooth muscle cells by depletion of GGPP

As blood pressure may be regulated by VSMCs contraction (30), the low blood pressure of GGPPS KO mice prompted us to examine the contractile properties of artery smooth muscle. To our surprise, for the mesentery from 7 week-old mice, the contractile responses to KCl depolarization and agonists (NE, norepinephrine and U46619) were almost abolished (Fig. 2*G*). Smooth muscle contraction is dependent on the expression of contractile proteins such as SMA, smooth muscle myosin heavy chain (SMMHC) and calponin. Immunofluorescent staining with anti-SMA antibody showed no expression of contractile proteins in the 7 week-old mutant aorta (Fig. 3*C*). More surprisingly, there were no DAPI signal in smooth muscle layer, indicating no smooth muscle cells existed within the tissue (Fig. 3*C*). HE staining also supported this conclusion (Fig. 3*E*). To find the point at which the smooth muscle cells started to decrease, we tested the aorta smooth muscle morphology at diverse age. Before 3 weeks after birth, the mutant aorta tissues had normal smooth muscle cells and regular elastic lines, while the mutant aorta from 3-week old mice had less smooth muscle cells and the elastic lines between muscle layers became straight. At 7 weeks after birth, almost no smooth muscle cells were observed and the elastic lines were straightened entirely (Fig. 3, *E* and *F*). To test whether there was a problem with smooth muscle development, we also tested mesentery contraction function at 4 weeks old. Upon respective treatment with KCl depolarization and norepinephrine (NE), the mesentery from 4 week-old KO mice developed significantly smaller force in contrast to CTR mice (KCl: KO: 1.641±0.35 mN *vs* CTR: 2.463±0.425 mN, p<0.005; NE: KO:1.78±0.662 mN *vs* CTR 2.98 ±0.237 mN, p<0.01). A similar inhibitory effect was also observed when the muscle was treated with U46619 (Fig. 3*A*). The corresponding reduction proportion of contraction function with smooth muscle cells decrease suggests a progressive loss of smooth muscle cells in aorta, which is well consistent with the force development.

3

To characterize the cell death, we measured the broken DNAs with TUNEL method and the proteins expression of LC3-II, GASDME and GASDMD by Western blot. By 3 weeks after birth, the smooth muscle cells of the mutant aorta had a clear broken DNA signal (Fig. 3*D* and Fig. S2*A*). LC3-II expression both in whole cell and mitochondria fractions (Fig. S2*B*) were significantly increased. As no GASDMD/GASDME were expressed in aorta smooth muscle (Fig. S2*C*), the death of the mutant VSMCs was attributable to apoptosis mixed with mitophagy, rather than to pyroptosis.

We then measured the rescue effect of exogenous GGPP *in vitro*. Firstly, we isolated smooth muscle cells from 2-week old mice and cultured *in vitro*. The CTR cells grew rapidly from the 4th -5th day, while the mutant cells died gradually (Fig. 4*A*). Upon addition of GGPP to the culture medium, the mutant cells displayed a comparable morphology to CTR, although the growth velocity was relatively slow (Fig. 4*A* and *B*). In addition, all these rescued cells were SMA and SMMHC positive (Fig. 4*C*). These results strongly suggested that the apoptosis of the mutant cells was contributed by GGPP depletion. However, the primary cells of the mutant jejunum, airway and bladder smooth muscles grew in a similar manner of CTR cells (Fig. S3, *A-F*). This phenomenon may be explained as that these smooth muscles might be not sensitive to GGPPS deletion due to heterogeneous metabolic patterns. However, the relative low KO efficiency of GGPPS in these tissues might be contribute to this differential sensitivity also (Fig. 2*B* and *C*).

GGPPS-deficient vascular smooth muscle displays inflammation responses along with abnormal eicosanoids production

To determine the gene expressive profile after GGPPS deletion, we subjected the GGPPS-deficient aorta tissue of 3-week old mice to RNA-seq analysis. Among 1668 genes with more than 3-fold altered expression, 1013 genes were up-regulated and 655 genes were down-regulated. GOTERM function analysis showed that these genes involved 537 pathways or physiological processes. Interestingly, most of them related to innate immunity or inflammation such as the response to virus, neutrophil chemotaxis, interferon beta and pro-inflammatory cytokines (e.g. IL-6, IL-1 and TNF) (Fig.

5, *A-C*). This result indicated an apparent metaflammation phenotype after GGPPS deletion. BIOCARTA analysis showed that the altered genes involved cell cycle, eicosanoid metabolism, multiple-drug resistance factors, p53 signaling pathway, classical complement pathway, neutrophil markers and Ras-independent pathway in NK cell-mediated cytotoxicity (Fig. 5*D*). To further validate the alteration of eicosanoids metabolism, Q-PCR assay were performed. As expected, the expressions of *Ptgs-1*(also called *Cox-1*), *Cyp2c5* and *Ptgs-2* (also called *Cox-2*) were changed in the same pattern with RNA-seq results (Fig. S4). As eicosanoids are closely related to inflammatory responses (31-36), the metaflammation occurring in the mutant cells may be primarily contributed by the abnormal eicosanoids production.

To know how eicosanoids metabolism changed, we then examined by LC-MS method the metabolic products of 53 liposomes related to eicosanoids metabolism. Orthogonal partial least-squares discriminant analysis (O-PLS-DA) was initially applied to LC-MS data to illustrate separation between KO and control individuals (Fig. 6*A*). The S-plot highlighted 4 metabolites significantly correlated with GGPPS deficiency (LTB4, LTE4, PGE1, LXA5) (Fig. 6*B*). These dimensionality-reduction analyses showed that the metabolites production were significantly changed in GGPPS-deficient aorta smooth muscle (Fig. 6, *A* and *B*) by their change in abundance (Fig. S5). In GGPPS-deficient smooth muscle, such fatty acids as eicosapentaenoic acid (EPA), docosahexaenoic acid (DHA) and arachidonic acid (AA) were accumulated significantly (Fig. 6*C*). Particularly, AA and its intermediate products were elevated apparently, e.g. LTB4 and LTE4 produced by 5-lipoxygenases (LOXs) were elevated about ~4 fold; the 19 r-hydroxy-5z, 8z, 11z, 14z-eicosatetraenoic acid (19-HETE) catalyzed by cytochrome P450 (CYP450) were elevated about ~2 folds; the epoxyeicosatrienoic acids produced by CYP450 including 14,15-EET, 11,12-EET, 8,9-EET and 5,6-EET were elevated about ~1.7 folds. The increased liposomes were reported to show pro-inflammatory tendency such as chemotaxis of LTB4 (37) and enhanced vascular permeability by LTE4 (38). Therefore, the accumulation of fatty acids or eicosanoids and their bioactive intermediates

4

implies an impairments of eicosanoids metabolism and hence induce inflammation and apoptosis (39).

Given the accumulated eicosanoids are a pathogenic factor for the inflammation and apoptosis, the neonatal animals in a suckling period would be expected more sensitive to GGPPS deletion because abundant polyunsaturated fatty acids were existed in mother milk(40), whereas the adult animal would be resistant to GGPPS deletion. To validate this expectation, we crossed $Ggps1^{flox/flox}$ mice with SM22-CreERT2 mice and then examined the phenotypes of adult ($Ggps1^{SM22KO}$) mice. After induction with tamoxifen for a week, GGPPS protein level in aorta smooth muscle was reduced less than 10% of CTR. However, the survival rate, appearance and body weights were not altered as we expected. The histology and contractile property of the mutant artery smooth muscle appeared normal also (Fig. S6, *A-F*).

GGPP mediates CYB5R3 translocation from mitochondria to ER through catalyzing CYB5R3 prenylation

To test if the abnormal eicosanoid production were caused by protein prenylation, we examined the amino acid sequence of the proteins associated with eicosanoids metabolism, and found only CYB5R3 contained a CAAX motif in C-terminal. CYB5R3 is a reductase using NADH and plasma membrane CoQ as substrates, and serves as a key component of the trans-membrane redox system (41,42), which is necessary for redox homeostasis and fatty acids metabolism (43). If CYB5R3 is responsible for the apoptosis of GGPPS-deficient smooth muscle cells, inhibition of CYB5R3 activity should cause smooth muscle apoptosis also. PTU (propylthiouracil) is a specific (44) and weak inhibitor of CYB5R3 (IC50= ~ 275 μM), and 0.25 mM PTU is sufficient to cause a significant decrease in enzyme activity (45,46). We treated the primary aorta smooth muscle cells with PTU from 1 μM to 100 μM. Expectedly, after incubated with CYB5R3 inhibitor PTU, the primary aorta smooth muscle cells died in a dose-dependent manner (Fig. 7*A*). We also compared the effect of PTU on A7R5 and primary aorta (ASMC) smooth muscle cells, and non-muscle cells including CHO cells, RAW 264.7 cells, L929 cells and 293T cells. 100 μM PTU induced a significant cell death of ASMC and A7R5 smooth muscle, a mild cell death of CHO and RAW 264.7 cells, and

no cell death of L929 and 293T cells, implying that smooth muscle was a preferential target of PTU (Fig. S7*A-F*).

Interestingly, in GGPPS-deficient aorta, the expression of total CYB5R3 protein was elevated (Fig. 7, *B* and *C*), possibly reflecting a compensatory effect secondary to the translocation failure of CYB5R3 as described below. As commercial anti-CYB5R3 antibody just recognize total CYB5R3 protein, we cannot determine if CYB5R3 was the substrate of GGPP directly. To address this, we made a specific antibody against non-prenylated CYB5R3 (anti-NP-CYB5R3) by immunizing mice with recombinant GST protein fusing with three CAAX motifs of CYB5R3 (Fig. 7*D*). To test the specificity of anti-NP-CYB5R3 antibody, we applied A7R5 cells transfected with *Cyb5r3* siRNA to Western blot assay. After *Cyb5r3* siRNA transfection, the signal produced by anti-NP-CYB5R3 antibody was reduced in the same manner as anti-total-CYB5R3 (Fig. 7*E*). Thus, anti-NP-CYB5R3 appears able to recognize CYB5R3 specifically.

As prenylation enabled protein to anchor on membrane, we then measured CYB5R3 distribution in the subcellular fractions of A7R5 smooth muscle cells. To our surprise, NP-CYB5R3 was exclusively detected in the mitochondria fraction, whereas total CYB5R3 existed both in mitochondria and plasma membrane (Fig. 7*G*). Treatment with HMGCR inhibitor simvastatin reduced CYB5R3 protein in membrane (Fig. 7, *F* and *G*). Therefore, this observation indicated that NP-CYB5R3 was pooled exclusively at mitochondria, while prenylated CYB5R3 was pooled at microsome. As microsomal fraction mainly reflects ER components, the prenylated CYB5R3 is primarily translocated to ER, the main site for eicosanoids metabolism.

DISCUSSION

Although metaflammation is contributed by singaling networks and involved by tremendous inflammatory cytokines and mediators (2), which aetiological factor triggers this inflammation process remains to be determined. In this report, by measuring the role of MVA intermediates in smooth muscle cells, we here found that the inhibition of GGPP led to inflammation through altered production of proinflammatory cytokines, eicosanoids and other mediators. In light of the facts that MVA or cholesterol biosynthesis is

5

highly affected by other metabolic pathways, such as glycolysis and fatty acid oxidation (47,48), our finding suggests that affected MVA pathway may be the etiological pathway triggering metaflammation, in which GGPP serves as a key causal link module. This finding is particularly useful for development of new anti-metaflammation drugs because it avoids applying multiple targets (49).

This linkage was accomplished by catalyzing CYB5R3 prenylation that was necessary for translocating it from mitochondria to ER. The prenylated CYB5R3 served to necessary for eicosanoids metabolism (50). As far as our knowledge, CYB5R3 mediate fatty acids elongation and desaturation within the microsomal eicosanoids metabolism. PUFAs (e.g. AA, EPA, DHA, and linoleic acid) are oxidized by COX, LOX or CYP450, in which CYB5R3 serves as an electron transfer and maintains oxidation/reduction homeostasis of ER (41,51,52). When CYB5R3 is absent or disrupted, the abnormal production of fatty acids is thus induced, which may be sufficient to induce apoptosis of smooth muscle cells. Indeed, CYB5R3 directly participates in CYP-450-mediated hydroxylation, and its absence leads to decreased production of 20-HETE (53). Therefore, our result not only uncovered a regulatory effect of MVA pathway on metaflammation, but also revealed a coupled regulation of between MVA pathway and eicosanoids metabolism. Moreover, it is also helpful to understand the preferential effect of statin drugs on vascular smooth muscle.

According to our observations, we proposed a working model (Fig. 8) for MVA pathway in regulation of inflammation. When mevalonate is produced by ER-docking HMG-CoA, MVA pathway starts with the participation of mevalonate kinase. As an important member of isoprenoids, GGPP is synthesized by GGPPS in cytoplasm, and GGTase I/II transfer the resultant GGPP to CYB5R3. The prenylated CYB5R3 translocate from mitochondria outer membrane to ER. The ER-resident CYB5R3 serves to maintain ER oxidation/reduction balance necessary for such eicosanoids synthesis as microsomal metabolism, or directly participate the metabolic reactions. When MVA pathway is inhibited, CYB5R3 prenylation was ablated and the bioactive intermediate metabolites or substrates of eicosanoid metabolism were accumulated, resulting in metaflammation and death (31,33-35).

The more interesting finding was that GGPP depletion was specific detrimental to neonatal mice but not to adult mice. This phenomenon may be explained as that the adult smooth muscle cells of the inducible KO animals is not sensitive to the MVA dysfunction, while perinatal smooth muscle does not, because 1) the accumulated lipid acids from breast milk are toxic to the SMC when they are not metabolized properly (40) ; 2) the perinatal SMC requires a large amount of new membrane that is primarily synthesized by cholesterol or MVA pathway.

The *Cyb5r3* gene encodes for two isoforms in which the soluble isoform is exclusively expressed in erythrocytes and the membrane-bound isoform is expressed in all cells (54,55). The latter contains a short amino acid sequence (MGAQLSTL), which can be myristoylated and thereby anchoring at membrane. Previous observations have showed that this myristoylated protein simultaneously anchors at outside of mitochondria and ER (55), but the differences existing between the mitochondria and ER forms are not known. Using a specific antibody against NP-CYB5R3, we here found that the NP-CYB5R3 anchored at mitochondria only, while the prenylated CYB5R3 anchored at ER. It means that the N-myristoylation event pools CYB5R3 protein at mitochondria, while their further prenylation pools CYB5R3 at ER. This finding uncovered a novel subcellular translocation model of CYB5R3.

In summary, we revealed a mechanistic linkage of MVA with metaflammation and a coupled regulation coordinating MVA with eicosanoids metabolism. The regulatory mechanism underneath involves CYB5R3 prenylation of GGPP that is necessary for microsomal homeostasis and hence eicosanoids metabolism. MVA pathway or GGPP production is envisioned to be a prospective therapeutic target of metaflammation.

Materials and methods
Animals: GGPPS^{SMKO} mice
Floxed *Ggps1* (56) and SMA-Cre (tg) mice (57) were bread and maintained at the Model Animal Research Centre of Nanjing University. All animal procedures were performed according to the animal protocol approved by the Institutional Animal Care and Use Committee of the Model Animal

Research Center of Nanjing University. All the experiments used both male and female mice.

Primary mouse aorta smooth muscle cells (SMCs) culture and cell treatment experiment

Primary mouse aorta SMC were prepared from 2-week-old mice and cultured as previously described (26). Briefly, aorta was isolated in HT buffer (137.0 mM NaCl, 2.7 mM KCl, 1.8 mM $CaCl_2$, 1 mM $MgCl_2,6H_2O$, 5.6 mM D-glucose, and 10 mM HEPES, pH 7.4) and cut longitudinally. All of the following experiments should be performed aseptically. After being washed in D-Hanks solution (8 g/L NaCl, 0.0475 g/L Na_2HPO_4, 0.35 g/L $NaHCO_3$, 0.4 g/L KCl, 0.06 g/L KH_2PO_4), the aorta was cut into small cubes and then digested 2 mg/mL collagenase I (WLS004196, Worthington, USA) in a 37°C water bath for 30 min. After being centrifuged at 300g for 3min, the tissue pellets were then digested in 2 mg/mL collagenase II (17101015, Gibco) and 0.5 mg/mL elastase (A002290, Worthington). After being centrifuged at 1000rpm for 3min, the cell pellets were expanded in high glucose DMEM containing 10% FBS (fetal bovine serum, Life Technologies), 100 units/ml penicillin and 100 mg/ml streptomycin and then incubated at 37°C. For GGPP rescue experiment, 10 uM GGPP (G6025, Sigma) was added into culture medium once the primary cells were cultured. 1-100 µM propylthiouracil (S1988, Selleck) were incubated with primary aorta SMCs.

Q-PCR assay

Quantitative RT-PCR was performed as described previously (30,58). Briefly, total RNA was extracted from C57BL/6J mice aorta using RNAiso Plus (Takara Bio). Then, 1 µg total RNA was reversely transcribed with the HiScript® Q RT SuperMix (Vazyme, R123) according to the manufacturer's instructions. Real-time quantitative qPCR was performed using the ABI Prism Step-One system with AceQ® qPCR SYBR® Green Master Mix (Vazyme, R141). The primers for target genes are listed in Extended Data Table 2. The *36b4* was as reference gene.

Western blot analysis

Tissue was homogenized in modified RIPA (50 mM Tris HCl, pH7.4; 1% NP-40, 0.25% Na deoxycholate, 150 mM NaCl,

1 mM EDTA) supplemented with 1x proteinase inhibitor cocktail (Roche, Switzerland). Protein was quantified with BCA protein assay kit and then loaded to SDS-PAGE and transferred to a PVDF membrane. The membrane was blocked with 5% BSA at RT for 1h and then incubated sequentially with primary and secondary antibodies. The primary antibodies include anti-GGPPS antibody (1:1000, ab155584, Abcam), anti-insulin receptor (1:2000, sc57342, Santa), anti-GASDMD antibody (1:1000, ab209845, Abcam), anti-GASDME antibody (1:1000, ab215191, Abcam), anti-β-actin (1:10000, AC15, Sigma-Aldrich), anti-GAPDH (1:5000, #2133, Signalway), anti-CYB5R3 (1:1000, PA5-36492, Thermo Fisher and 10894-1-AP, Proteintech) and home-made anti-NP-CYB5R3 antibody (1:1000). The signals were visualized with ECL (Sudgen biotech, China)).

Blood pressure recording

Blood pressure of mice was measured with noninvasive tail-cuff method as previously described (26). The mice were fixed in a plastic box on a 37°C thermostatic blanket. The pulse sensor was placed under the tail of mice (ALC-NIBP system, Shanghai Alcott Biotech, China). Each mouse took 5 min as adaptation and was measured for 20 cycles with 35-s intervals every day at the regular time. The first 5-7 days were as training for mice to get stable recordings. The systolic blood pressure (SBP) and diastolic blood pressure (DBP) of later 5-7 days was statistical.

Immunofluorescence

The isolated aorta tissues were fixed in 4% PFA (paraformaldehyde) and then embedded into OCT (optimum cutting temperature). The tissues were then sliced into 10 µm and incubated with primary antibodies and then incubated with respective secondary antibodies and DAPI (Biosharp, China). The sections were mounted with 50% glycerol and examined under a Zeiss LSM880 confocal microscope (Zeiss, Germany). The primary antibody is mouse anti-SMA (#MS-113-P1, Thermo Fisher Scientific) and rabbit anti-SMMHC (ab53219, Abcam).

Morphologic

Aorta, mesentery, jejunum, airway, bladder, liver, heart were isolated and fixed in 4% PFA at 4°C overnight. After ethanol

7

gradient dehydration, the tissues were embedded in paraffin wax and sectioned at a thickness of 5 μm for followed HE (hematoxylin and eosin) stain.

Force measurement of mesentery

Mesentery segments were isolated and subjected to force measurement according to previous method (59). Briefly, a segment with length of 1.4 mm was prepared and threaded by two steel wires (40 mm in diameter). The steel wires were then mounted in myograph chamber (610-M; Danish Myo Technology, Aarhus, Denmark), which contained HT buffer at constant 37°C. Before stimulated with 124 mM KCl (15.7 mM NaCl, 124.0 mM KCl, 1.8 mM $CaCl_2$, 1 mM $MgCl_2$,$6H_2O$, 5.6 mM D-glucose, and 10 mM HEPES, pH 7.4), the segment was equilibrated in optimal resting tension for 30 min. After washing with HT buffer, the segments were than stimulated with 10 uM norepinephrine (NE) (74490, Sigma) or 0.1 uM U46619 (D8174, Sigma). All forces were persistent for 10 min and recorded on a recording device (AD Instruments, Australia). The data was acquired and analyzed with Lab Chart 5 program.

Apoptosis detection

Aorta frozen sections were subjected to TUNEL BrightGreen Apoptosis Detection Kit (A112, Vazyme) following the manufacturer's instructions. The cell nuclear was stained with DAPI.

Cell proliferation assay

10 uL CCK-8 (20148, Sudgen biotech, China) was added to each well of cells and incubated at 37°C for 4 h. Absorbance values at 450 nm and 650 nm were recorded using a microplate reader (BioTek synergy microplate reader, USA).

Mitochondria isolation

Mitochondria of aorta were isolated as previously described (58). Briefly, aorta was minced and homogenized, and then centrifuged at 600 g at 4°C for 15 min twice. The resultant supernatants were centrifuged twice at 8,000 g at 4°C for 15 min and the pellet was suspended in MIM buffer (300 mM sucrose, 10 mM Na-HEPES, 0.2 mM EDTA, pH 7.2).

A7R5 cell culture and siRNA of Cyb5r3

Double-stranded siRNA targeting rat *Cyb5r3* were synthesized (GenePharma, China) with the following sequences: sense, 5- GGAAAUGAAAGGUAAACAG UU-3 and antisense, 5- CUGUUUACCUUUCAUUUCC UU-3. When cell density was up to $1×10^6$, 30 nM siRNAs of CYB5R3 or NC were transfected into A7R5 cells using Nucleofection™ 2b (lonza, Switzerland) with program X-001 according to the manufacturer's instructions. Cells were lysed with modified RIPA after 48 h and 72 h for proteins extraction. For subcellular fractionation experiment, 10 μM simvastatin (S1792, Selleck) were added to culture medium.

RNA-seq analysis

Transcriptomics analysis of 3 weeks old mice were performed as described previously (58). Total RNA was isolated from the aorta using RNAiso Plus (Takara Bio). 2 ug total RNA was sent to commercial company Novogene (China) for RNA-sequencing. Two independent KO samples versus CTR mice were analyzed. Paired-end, 150 nt reads were obtained on an Illumina X Ten from the same sequencing lane. The sequencing data were initially processed by Trimmomatic 0.36 and then aligned to the mouse genome UCSC mm10. The aligned results were further assembled using TopHat 2.0.14 with the default parameters and calculated Fragments Per Kb of exon per Million mapped reads (FPKM) using Cufflinks 2.2.1. Gene expression with FPKM < 1 were excluded in both CTR and KO. The genes of KO fold changed more than 3-fold compared to CTR and the significant P-value (< 0.05) (a total of 1688 genes) were uploaded into DAVID Bioinformatics Resources 6.8 (https://david.ncifcrf.gov) to GOTERM analysis and BIOCART analysis.

Lipidosome metabolomics analysis

Aorta samples were sent to commercial company Metware (Wuhan, china) for lipidosome metabolomics analysis according to the company's official experimental method. Briefly, all experiments were performed on ice. 50 mg sample and 1 steel ball were added to 1mL methanol. After homogenization for 1-2 min, the steel ball was carefully removed. The samples were whirled for 5 min and then kept still. 10 uL of 1 uM internal standard mixture was added to each sample and vortex for 10 min. After centrifuge at 5000

rpm for 10 min at 4°C, the supernatant was blown dry with N_2 and vortex with 4 mL 10% methanol-water mixture. After SPE Column (C18 column) was activated, acid sample was obtained through pH adjustment and quickly added to the SPE Column. The target samples were eluted and collected. The collected samples were blown dry with N_2 and then vortex in 100 uL methanol-water (v:v=1:1) for 30s. The supernatants were then analyzed in Ultra Performance Liquid Chromatography (UPLC, Shim-pack UFLC SHIMADZU CBM30A) and Tandem mass spectrometry (MS/MS, Applied Biosystems QTRAP). The absolute concentration of target metabolite were calculated based on the standard curves.

Preparation of anti-NP-CYB5R3 (292-301) antibody

Anti-NP-CYB5R3 (292-301) antibody was prepared as previously described (60). Briefly, GGCCATCCCAAGGAGCGATGCTTCACCTTCGGTGG TGGTGGCCATCCCAAGGAGCGATGCTTCACCTTCG GTGGTGGTGGCCATCCCAAGGAGCGATGCTTCACC TTCGGTGGTGGTTAA was inserted into pGEX6P-3 vector through *Bam*H I and *EcoR* I. GST–CYB5R3 (292-301) was expressed in *E. coli* BL21 (DE3) cells after induced with 0.1 mM IPTG. GST–CYB5R3 (292-301) protein was purified with Glutathione Sepharose 4B (17-0756-01, GE Healthcare) using the gravity flow method according to the manufacturer's instructions. Protein concentrations were measured with a Bio-Rad protein assay kit (500-0006, Bio-Rad). The recombinant protein mixed with Freund's adjuvant (Complete: F5881, sigma; Incomplete: F5506, sigma) was intraperitoneal injected to BALB/c mice for antibody production.

Subcellular fractionation

A7R5 cells were scraped in 500 μL subcellular fractionation buffer (HEPES, pH 7.4, 20 mM; KCl, 10 mM; $MgCl_2$, 2 mM; EDTA, 1 mM; EGTA, 1 mM; DTT, 1 mM) and 1x proteinase inhibitor cocktail (Roche, Switzerland) (61). The ice-cold samples were centrifuged at 3,000 rpm at 4°C for 5 min, and subjected the supernatant for a further centrifugation at 8,000 rpm at 4°C for 5 min. The pellet containing mitochondria was washed with 500 uL subcellular fractionation buffer for 1 time and lysed in 100 uL TBS/0.1% SDS. The supernatant

was transferred to a new tube and centrifuged in an ultracentrifuge at 40,000 rpm at 4°C for 1.5 h. The pellet (membrane fraction) was lysed in 100 uL TBS/0.1% SDS. The proteins in all fractions were analyzed by Western blot.

Animals: GGPPS^SM22KO Mice

The protocol was referred to previously description (62). Floxed *Ggps1* mice were crossed with SM-CreERT2 (ki) mice whose Cre recombinase is driven by SM22 promoter. The gene deletion was induced by i.p. injection with tamoxifen (100 uL 10 mg/ml, Sigma, T5648) for five consecutive days at 5-week old. 100 mg tamoxifen was dissolved in 0.5 ml ethanol at 55°C and then added with 9.5 ml sunflower oil and then aliquot and stored at -80°C.

Primary Jejunum SMC Culture

Primary mouse jejunum SMC were prepared from 2-week-old mice and cultured as previously described (62). The mesentery and adipose tissues were removed. Smooth muscles were carefully teased away from the epithelium. The muscle layers were washed in D'-Hanks for 5 times and then cut about 300 times in DMEM with 10% FBS and then digested in 2 mg/mL collagenase II (17101015, Gibco) in a 37°C water bath for 30 min. After centrifuged at 1000 rpm for 5 min, jejunum SMCs were cultured in DMEM with 10% FBS, 100 units/ml penicillin and 100 mg/ml streptomycin and then incubated at 37°C.

Primary Airway SMC Culture

2-week-old mice were sacrificed by cervical dislocation. Trachea and extra-pulmonary bronchus were isolated and removed connective tissues and cartilage thoroughly. Airway smooth muscle was cut and washed in D'-Hanks for 5 times. The muscle was then cut about 300 times in DMEM with 10% FBS, 2 mg/mL collagenase I (WLS004196, Worthington) and 1.5 mg/mL trypsin (TB0627, BBI) and digested in 37°C water bath for 30 min. After centrifuged at 1000 rpm for 5 min, airway SMCs were cultured in DMEM with 10% FBS, 100 units/ml penicillin and 100 mg/ml streptomycin at 37°C.

Primary Bladder SMC Culture

2-week-old mice were killed by cervical dislocation (63). Bladder was isolated. The vessel and related tissues were

9

removed. The smooth muscle layers were teased away from epithelium carefully and washed in D'-Hanks for 5 times. The muscle were then cut 300 times in DMEM with 10% FBS and 2 mg/mL collagenase IV (Gibco, 17104019) and 2 mg/mL Dispase II (13783200, Roche) and digested in 37°C water bath for 40 min. After centrifuged at 1000 rpm for 5 min, bladder SMCs were cultured in DMEM containing 10% FBS, 100 units/ml penicillin and 100 mg/ml streptomycin and then incubated at 37°C.

Echocardiography

The echocardiography was measured using a Vevo 3100 High-Resolution *In Vivo* Micro-Imaging System (VisualSonics, Canada) according to the manufacturer's instructions. Briefly, the mice were settled on a 37°C platform after being anesthetized by isoflurane in gas form. The chest hair of the mice was removed with a depilatory cream. The degree of anesthesia was adjusted to obtain a stable heart rate of 350 ± 70 beats/min. M-mode echocardiography was gotten with RMV 30 mHz scan head.

Quantification and statistical analysis

The animal numbers used for all experiments are indicated in the corresponding figure legends. All values data were presented as means ± s.e.m. Two-tailed unpaired Student's T-test was applied on comparison of two groups (KO verse KO). ANOVA was applied on comparisons of multiple groups. OPLS-DA analysis was from commercial company Metware. All heatmap analysis were performed using the OmicShare tools, a commercial online platform for data analysis (http://www.omicshare.com/tools). Fold change analysis of eicosanoids metabolites was performed using Origin 2020b. The left statistical analysis was performed using GraphPad Prism 8 software. All quantification analysis of Western blot was performed using ImageJ software. For QPCR, RNA-seq and LC-MS l experiments of mice, n represents a samples composed of multiple mice. Statistical differences are indicated as * for $P < 0.05$, ** for $P<0.01$ and *** for $P<0.001$.

Data availability

The RNA-seq data generated in this study are available in the Gene Expression Omnibus repository under the accession number: GSE142820.

Conflict of interest

The authors declare that they have no conflicts of interest with the contents of this article.

References

1. Hotamisligil, G. S. (2006) Inflammation and metabolic disorders. *Nature* **444**, 860-867

2. Hotamisligil, G. S. (2017) Inflammation, metaflammation and immunometabolic disorders. *Nature* **542**, 177-185

3. Favier, L. A., and Schulert, G. S. (2016) Mevalonate kinase deficiency: current perspectives. *Appl Clin Genet* **9**, 101-110

4. Goldstein, J. L., and Brown, M. S. (1990) Regulation of the mevalonate pathway. *Nature* **343**, 425-430

5. McTaggart, S. J. (2006) Isoprenylated proteins. *Cell Mol Life Sci* **63**, 255-267

6. Zhang, F. L., and Casey, P. J. (1996) Protein prenylation: molecular mechanisms and functional consequences. *Annual review of biochemistry* **65**, 241-269

7. Clarke, S. (1992) PROTEIN ISOPRENYLATION AND METHYLATION AT CARBOXYL-TERMINAL CYSTEINE RESIDUES. *Annual Review of Biochemistry* **61**, 355-386

8. Farnsworth, C. C., Seabra, M. C., Ericsson, L. H., Gelb, M. H., and Glomset, J. A. (1994) Rab geranylgeranyl transferase catalyzes the geranylgeranylation of adjacent cysteines in the small GTPases Rab1A, Rab3A, and Rab5A. *Proceedings of the National Academy of Sciences of the United States of America* **91**, 11963-11967

9. Endo, A. (1992) The discovery and development of HMG-CoA reductase inhibitors. *Journal of Lipid Research* **33**, 1569-1582

10. Lane, K. T., and Beese, L. S. (2006) Thematic review series: lipid posttranslational modifications. Structural biology of protein farnesyltransferase and geranylgeranyltransferase type I. *J Lipid Res* **47**, 681-699

11. Jiao, Z., Cai, H., Long, Y., Sirka, O. K., Padmanaban, V., Ewald, A. J., and Devreotes, P. N. (2020) Statin-induced GGPP depletion blocks macropinocytosis and starves cells with oncogenic defects. *Proc Natl Acad Sci U S A* **117**, 4158-4168

12. Mullen, P. J., Yu, R., Longo, J., Archer, M. C., and Penn, L. Z. (2016) The interplay between cell signalling and the mevalonate pathway in cancer. *Nat Rev Cancer* **16**, 718-731

13. Jiang, S., Shen, D., Jia, W. J., Han, X., Shen, N., Tao, W., Gao, X., Xue, B., and Li, C. J. (2016) GGPPS-mediated Rab27A geranylgeranylation regulates beta cell dysfunction during type 2 diabetes development by affecting insulin granule docked pool formation. *J Pathol* **238**, 109-119

14. Tao, W., Wu, J., Xie, B.-X., Zhao, Y.-Y., Shen, N., Jiang, S., Wang, X.-X., Xu, N., Jiang, C., Chen, S., Gao, X., Xue, B., and Li, C.-J. (2015) Lipid-induced Muscle Insulin Resistance Is Mediated by GGPPS via Modulation of the RhoA/Rho Kinase Signaling Pathway. *The Journal of biological chemistry* **290**, 20086-20097

15. Chen, W. B., Lai, S. S., Yu, D. C., Liu, J., Jiang, S., Zhao, D. D., Ding, Y. T., Li, C. J., and Xue, B. (2015) GGPPS deficiency aggravates CCl4-induced liver injury by inducing hepatocyte apoptosis. *FEBS Lett* **589**, 1119-1126

16. Yeh, Y. S., Jheng, H. F., Iwase, M., Kim, M., Mohri, S., Kwon, J., Kawarasaki, S., Li, Y., Takahashi, H., Ara, T., Nomura, W., Kawada, T., and Goto, T. (2018) The Mevalonate Pathway Is Indispensable for Adipocyte Survival. *iScience* **9**, 175-191

17. Munoz, M. A., Jurczyluk, J., Mehr, S., Chai, R. C., Arts, R. J. W., Sheu, A., McMahon, C., Center, J. R., Singh-Grewal, D., Chaitow, J., Campbell, D. E., Quinn, J. M. W., Alexandrov, K., Tnimov, Z., Tangye, S. G., Simon, A., Phan, T. G., and Rogers, M. J. (2017) Defective protein prenylation is a diagnostic biomarker of mevalonate kinase deficiency. *J Allergy Clin Immunol* **140**, 873-875 e876

18. Munoz, M. A., Jurczyluk, J., Simon, A., Hissaria, P., Arts, R. J. W., Coman, D., Boros, C., Mehr, S., and Rogers, M. J. (2019) Defective Protein Prenylation in a Spectrum of Patients With Mevalonate Kinase Deficiency. *Front Immunol* **10**, 1900

19. Takata, R., Fukasawa, S., Hara, T., Nakajima, H., Yamashina, A., Yanase, N., and Mizuguchi, J. (2004) Cerivastatin-induced apoptosis of human aortic smooth muscle cells through partial inhibition of basal activation of extracellular signal-regulated kinases. *Cardiovascular Pathology* **13**, 41-48

20.	Erl, W. (2005) Statin-induced vascular smooth muscle cell apoptosis: a possible role in the prevention of restenosis? *Curr Drug Targets Cardiovasc Haematol Disord* **5**, 135-144

21.	Erl*, W. (2005) Statin-induced Vascular Smooth Muscle Cell Apo.pdf. *Current Drug Targets - Cardiovascular & Haematological Disorders*

22.	Knapp, A. C., Huang, J., Starling, G., and Kiener, P. A. (2000) Inhibitors of HMG-CoA reductase sensitize human smooth muscle cells to Fas-ligand and cytokine-induced cell death. *Atherosclerosis* **152**, 217-227

23.	Glorioso, N., Troffa, C., Filigheddu, F., Dettori, F., Soro, A., Parpaglia, P. P., Collatina, S., and Pahor, M. (1999) Effect of the HMG-CoA Reductase Inhibitors on Blood Pressure in Patients With Essential Hypertension and Primary Hypercholesterolemia. *Hypertension* **34**, 1281-1286

24.	Ferrier, K. E., Muhlmann, M. H., Baguet, J.-P., Cameron, J. D., Jennings, G. L., Dart, A. M., and Kingwell, B. A. (2002) Intensive cholesterol reduction lowers blood pressure and large artery stiffness in isolated systolic hypertension. *Journal of the American College of Cardiology* **39**, 1020-1025

25.	Borghi, C., Dormi, A., Veronesi, M., Immordino, V., and Ambrosioni, E. (2002) Use of Lipid-Lowering Drugs and Blood Pressure Control in Patients With Arterial Hypertension. *Journal of clinical hypertension (Greenwich, Conn.)* **4**, 277-285

26.	Sun, J., Tao, T., Zhao, W., Wei, L., She, F., Wang, P., Li, Y., Zheng, Y., Chen, X., Wang, W., Qiao, Y., Zhang, X. N., and Zhu, M. S. (2019) CPI-17-mediated contraction of vascular smooth muscle is essential for the development of hypertension in obese mice. *J Genet Genomics* **46**, 109-118

27.	Lin, C. S., Hsieh, P. S., Hwang, L. L., Lee, Y. H., Tsai, S. H., Tu, Y. C., Hung, Y. W., Liu, C. C., Chuang, Y. P., Liao, M. T., Chien, S., and Tsai, M. C. (2018) The CCL5/CCR5 Axis Promotes Vascular Smooth Muscle Cell Proliferation and Atherogenic Phenotype Switching. *Cell Physiol Biochem* **47**, 707-720

28.	Bundy, J. D., Li, C., Stuchlik, P., Bu, X., Kelly, T. N., Mills, K. T., He, H., Chen, J., Whelton, P. K., and He, J. (2017) Systolic Blood Pressure Reduction and Risk of Cardiovascular Disease and Mortality: A Systematic Review and Network Meta-analysis. *JAMA Cardiol* **2**, 775-781

29.	Huynh, K. (2017) Hypertension: Very low achieved SBP increases risk of cardiovascular death. *Nat Rev Cardiol* **14**, 316-317

30.	Qiao, Y. N., He, W. Q., Chen, C. P., Zhang, C. H., Zhao, W., Wang, P., Zhang, L., Wu, Y. Z., Yang, X., Peng, Y. J., Gao, J. M., Kamm, K. E., Stull, J. T., and Zhu, M. S. (2014) Myosin phosphatase target subunit 1 (MYPT1) regulates the contraction and relaxation of vascular smooth muscle and maintains blood pressure. *The Journal of biological chemistry* **289**, 22512-22523

31.	Esser-von Bieren, J. (2017) Immune-regulation and -functions of eicosanoid lipid mediators. *Biol Chem* **398**, 1177-1191

32.	Tunctan, B., Senol, S. P., Temiz-Resitoglu, M., Guden, D. S., Sahan-Firat, S., Falck, J. R., and Malik, K. U. (2019) Eicosanoids derived from cytochrome P450 pathway of arachidonic acid and inflammatory shock. *Prostaglandins Other Lipid Mediat* **145**, 106377

33.	Ramirez, M. U., Stirling, E. R., Emenaker, N. J., Roberts, D. D., and Soto-Pantoja, D. R. (2018) Thrombospondin-1 interactions regulate eicosanoid metabolism and signaling in cancer-related inflammation. *Cancer Metastasis Rev* **37**, 469-476

34.	Khan, S. A., and Jackson, R. T. (2018) Polyunsaturated fatty acids, inflammation, and metabolic syndrome in South Asian Americans in Maryland. *Food Sci Nutr* **6**, 1575-1581

35.	Delmastro-Greenwood, M., Freeman, B. A., and Wendell, S. G. (2014) Redox-dependent anti-inflammatory signaling actions of unsaturated fatty acids. *Annu Rev Physiol* **76**, 79-105
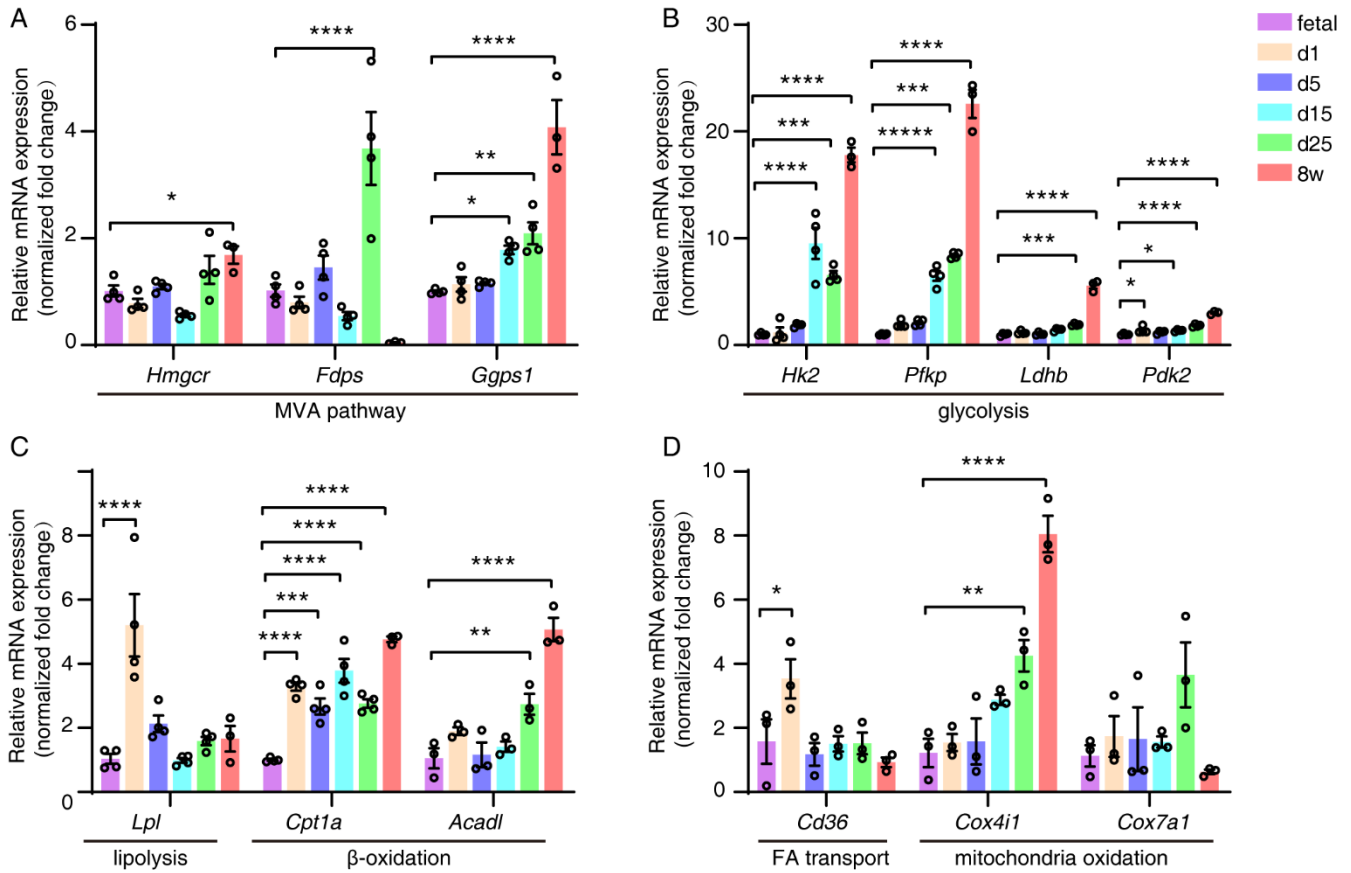
36. Wang, W., Yang, J., Zhang, J., Wang, Y., Hwang, S. H., Qi, W., Wan, D., Kim, D., Sun, J., Sanidad, K. Z., Yang, H., Park, Y., Liu, J. Y., Zhao, X., Zheng, X., Liu, Z., Hammock, B. D., and Zhang, G. (2018) Lipidomic profiling reveals soluble epoxide hydrolase as a therapeutic target of obesity-induced colonic inflammation. *Proc Natl Acad Sci U S A* **115**, 5283-5288

37. Lammermann, T., Afonso, P. V., Angermann, B. R., Wang, J. M., Kastenmuller, W., Parent, C. A., and Germain, R. N. (2013) Neutrophil swarms require LTB4 and integrins at sites of cell death in vivo. *Nature* **498**, 371-375

38. Chan, C. C., and Ford-Hutchinson, A. (1985) Effects of synthetic leukotrienes on local blood flow and vascular permeability in porcine skin. *J Invest Dermatol* **84**, 154-157

39. Song, Z., Huang, G., Chiquetto Paracatu, L., Grimes, D., Gu, J., Luke, C. J., Clemens, R. A., and Dinauer, M. C. (2020) NADPH oxidase controls pulmonary neutrophil infiltration in the response to fungal cell walls by limiting LTB4. *Blood* **135**, 891-903

40. Nilsson, A. K., Lofqvist, C., Najm, S., Hellgren, G., Savman, K., Andersson, M. X., Smith, L. E. H., and Hellstrom, A. (2018) Long-chain polyunsaturated fatty acids decline rapidly in milk from mothers delivering extremely preterm indicating the need for supplementation. *Acta Paediatr* **107**, 1020-1027

41. Villalba, J. M., Navarro, F., Córdoba, F., Serrano, A., Arroyo, A., Crane, F. L., and Navas, P. (1995) Coenzyme Q reductase from liver plasma membrane: purification and role in trans-plasma-membrane electron transport. *Proceedings of the National Academy of Sciences* **92**, 4887

42. Navarro, F., Villalba, J. M., Crane, F. L., Mackellar, W. C., and Navas, P. (1995) A Phospholipid-Dependent NADH-Coenzyme Q Reductase from Liver Plasma Membrane. *Biochemical and Biophysical Research Communications* **212**, 138-143

43. Martin-Montalvo, A., Sun, Y., Diaz-Ruiz, A., Ali, A., Gutierrez, V., Palacios, H. H., Curtis, J., Siendones, E., Ariza, J., Abulwerdi, G. A., Sun, X., Wang, A. X., Pearson, K. J., Fishbein, K. W., Spencer, R. G., Wang, M., Han, X., Scheibye-Knudsen, M., Baur, J. A., Shertzer, H. G., Navas, P., Villalba, J. M., Zou, S., Bernier, M., and de Cabo, R. (2016) Cytochrome b(5) reductase and the control of lipid metabolism and healthspan. *NPJ Aging Mech Dis* **2**, 16006-16006

44. Kariya, K., Lee, E., Yamaoka, M., and Ishikawa, H. (1984) Selective induction of cytochrome b5 and NADH cytochrome b5 reductase by propylthiouracil. *Life Sci* **35**, 2327-2334

45. Lee, E., and Kariya, K. (1986) Propylthiouracil, a selective inhibitor of NADH-cytochrome b5 reductase. *FEBS Lett* **209**, 49-51

46. Neve, E. P. A., Nordling, Å., Andersson, T. B., Hellman, U., Diczfalusy, U., Johansson, I., and Ingelman-Sundberg, M. (2012) Amidoxime Reductase System Containing Cytochromeb5Type B (CYB5B) and MOSC2 Is of Importance for Lipid Synthesis in Adipocyte Mitochondria. *Journal of Biological Chemistry* **287**, 6307-6317

47. Seo, E., Kang, H., Choi, H., Choi, W., and Jun, H. S. (2019) Reactive oxygen species-induced changes in glucose and lipid metabolism contribute to the accumulation of cholesterol in the liver during aging. *Aging cell* **18**, e12895

48. Gruenbacher, G., and Thurnher, M. (2017) Mevalonate Metabolism in Immuno-Oncology. *Front Immunol* **8**, 1714

49. Hotamisligil, G. S. (2017) Foundations of Immunometabolism and Implications for Metabolic Health and Disease. *Immunity* **47**, 406-420

50. Nakamura, M. T., and Nara, T. Y. (2004) Structure, function, and dietary regulation of delta6, delta5, and delta9 desaturases. *Annu Rev Nutr* **24**, 345-376

51. Heppard, E. P., Kinney, A. J., Stecca, K. L., and Miao, G. H. (1996) Developmental and growth temperature regulation of two different microsomal omega-6 desaturase genes in soybeans. *Plant physiology* **110**, 311-319

52. Tocher, D. R., Leaver, M. J., and Hodgson, P. A. (1998) Recent advances in the biochemistry and molecular biology of fatty acyl desaturases. *Progress in Lipid Research* **37**, 73-117

53. Hildebrandt, A., and Estabrook, R. W. (1971) Evidence for the participation of cytochrome b 5 in hepatic microsomal mixed-function oxidation reactions. *Arch Biochem Biophys* **143**, 66-79

54. Borgese, N., D'Arrigo, A., De Silvestris, M., and Pietrini, G. (1993) NADH-cytochrome b 5 reductase and cytochrome b 5 isoforms as models for the study of post-translational targeting to the endoplasmic reticulum. *FEBS Letters* **325**, 70-75

55. Leroux, A., Mota Vieira, L., and Kahn, A. (2001) Transcriptional and translational mechanisms of cytochrome b5 reductase isoenzyme generation in humans. *Biochem J* **355**, 529-535

56. Xu, N., Guan, S., Chen, Z., Yu, Y., Xie, J., Pan, F. Y., Zhao, N. W., Liu, L., Yang, Z. Z., Gao, X., Xu, B., and Li, C. J. (2015) The alteration of protein prenylation induces cardiomyocyte hypertrophy through Rheb-mTORC1 signalling and leads to chronic heart failure. *J Pathol* **235**, 672-685

57. He, W. Q., Peng, Y. J., Zhang, W. C., Lv, N., Tang, J., Chen, C., Zhang, C. H., Gao, S., Chen, H. Q., Zhi, G., Feil, R., Kamm, K. E., Stull, J. T., Gao, X., and Zhu, M. S. (2008) Myosin light chain kinase is central to smooth muscle contraction and required for gastrointestinal motility in mice. *Gastroenterology* **135**, 610-620

58. Fu, T., Xu, Z., Liu, L., Guo, Q., Wu, H., Liang, X., Zhou, D., Xiao, L., Liu, L., Liu, Y., Zhu, M. S., Chen, Q., and Gan, Z. (2018) Mitophagy Directs Muscle-Adipose Crosstalk to Alleviate Dietary Obesity. *Cell Rep* **23**, 1357-1372

59. Sun, J., Yang, G. M., Tao, T., Wei, L. S., Pan, Y., and Zhu, M. S. (2018) Isometric Contractility Measurement of the Mouse Mesenteric Artery Using Wire Myography. *J Vis Exp*

60. Tao, T., Sun, J., Peng, Y., Li, Y., Wang, P., Chen, X., Zhao, W., Zheng, Y. Y., Wei, L., Wang, W., Zhou, Y., Liu, J., Shi, Y. S., and Zhu, M. S. (2019) Golgi-resident TRIO regulates membrane trafficking during neurite outgrowth. *The Journal of biological chemistry* **294**, 10954-10968

61. Han, Y. M., Bedarida, T., Ding, Y., Somba, B. K., Lu, Q., Wang, Q., Song, P., and Zou, M. H. (2018) beta-Hydroxybutyrate Prevents Vascular Senescence through hnRNP A1-Mediated Upregulation of Oct4. *Mol Cell* **71**, 1064-1078 e1065

62. Chen, C., Tao, T., Wen, C., He, W. Q., Qiao, Y. N., Gao, Y. Q., Chen, X., Wang, P., Chen, C. P., Zhao, W., Chen, H. Q., Ye, A. P., Peng, Y. J., and Zhu, M. S. (2014) Myosin light chain kinase (MLCK) regulates cell migration in a myosin regulatory light chain phosphorylation-independent mechanism. *The Journal of biological chemistry* **289**, 28478-28488

63. Zupancic, D., Mrak Poljsak, K., and Kreft, M. E. (2018) Co-culturing porcine normal urothelial cells, urinary bladder fibroblasts and smooth muscle cells for tissue engineering research. *Cell Biol Int* **42**, 411-424

FOOTNOTES

The abbreviations used are: GGPPS, geranygeranyldiphosphate synthase; MVA, mevalonate pathway; CYB5R3, cytochrome b5 reductase 3; eicosapentaenoic acid, EPA; docosahexaenoic acid, DHA; arachidonic acid, AA; LTB4, leukotriene B4; LTE4, leukotriene E4; ER , endoplasmic reticulum; HMGCR, 3-hydroxy-3-methylglutaryl-Coenzyme A reductase; FPP, farnesyl diphosphate; GGTase I/II, geranylgeranyltransferase I /II; MKD, mevalonate kinase deficiency; VSMCs, vascular smooth muscle cells; Pfkp, Platelet phosphofructokinase; Ldhb, lactate dehydrogenase B; Pdk2, Pyruvate dehydrogenase kinase isoform 2; Lpl, lipolysis; Cpt1a, Carnitine Palmitoyltransferase 1A; Acadl, acyl-Coenzyme A dehydrogenase; Fasn, lipogenesis; Cox4i1, cytochrome c oxidase subunit 4I1; Cox7a1, Cytochrome c oxidase subunit 7A1; SMA, smooth muscle α-actin; NE, norepinephrine; SMMHC, smooth muscle myosin heavy chain; PTU, propylthiouracil; COX, cyclooxygenase; lipoxygenase; CYP450, Cytochrome P450.
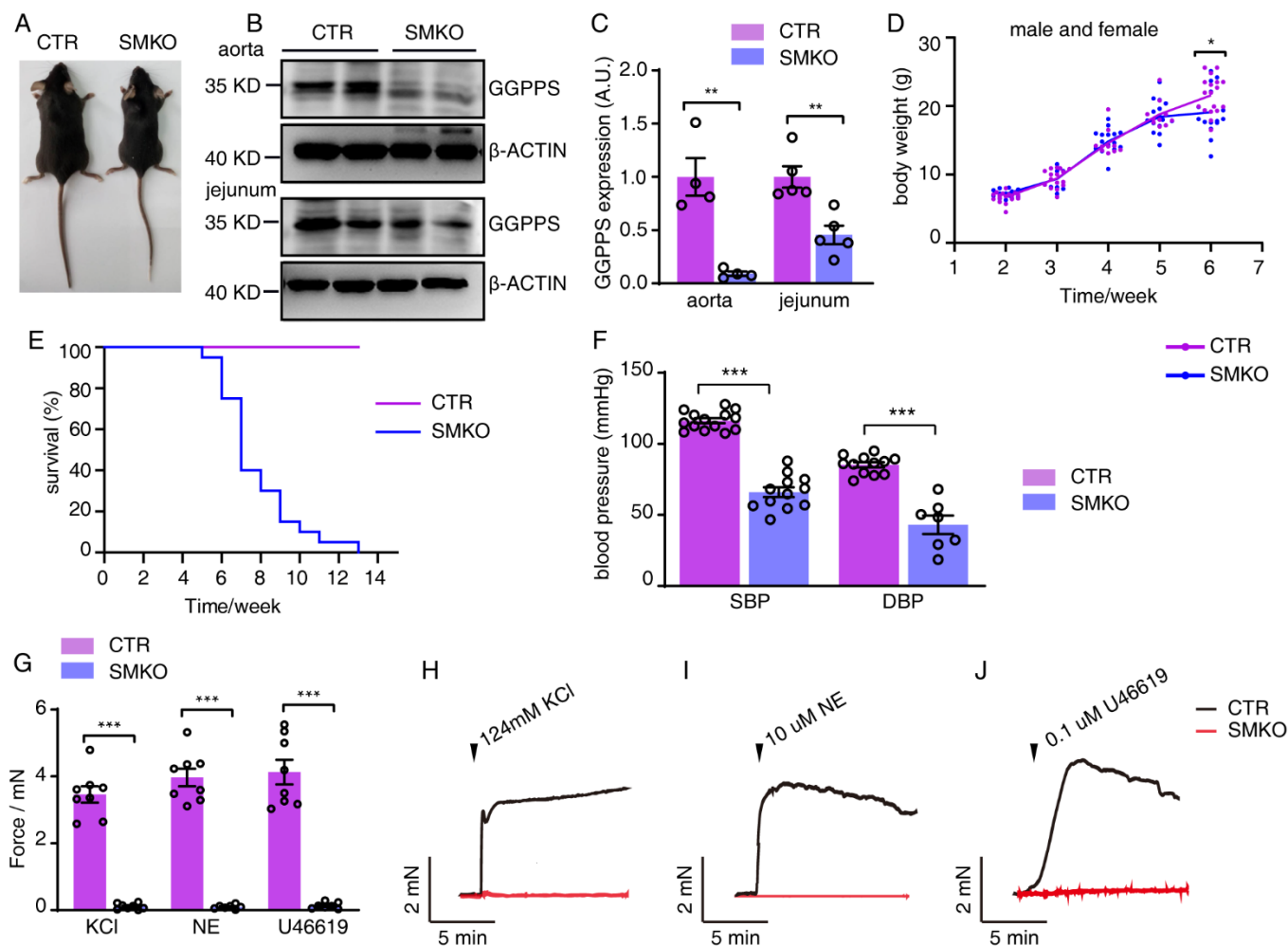
Figure 1. Dynamic expression of the genes associated with metabolism in aorta tissues. *A*, The relative mRNA levels of the genes associated with MVA pathway (n=4). *B*, relative mRNA levels of glycolysis-associated genes (n=4). *C*, relative mRNA levels of lipolysis- and β-oxidation-related genes (n=3). *D*, relative mRNA levels of the genes associated with fatty acids (FA) transport and mitochondria oxidation (n=4). The aorta tissues were isolated from C57BL/6 mice (E18.5 to 8 weeks) and subjected to a real-time PCR assay. Each n was composed of 2-9 mice. Relative mRNA levels were normalized to that of control group, respectively. All data are presented as mean ± s.e.m. of biologically independent samples with one-way ANOVA followed with Bonferroni's test. Error bar represents Bonferroni's multiple comparisons test compared with fetal *, $p<0.05$; **, $p<0.01$; ***, $p<0.001$; ****, $p<0.0001$. d1 means one day old.

Figure 2. Phenotypic characterization of GGPPS^SMKO mice. *A*, schematic representation of the *Ggps1* smooth muscle-specific knockout strategy. *B*, appearance of GGPPS^SMKO and CTR mouse. *C-D*, Western blot analysis of GGPPS protein in the aorta and jejunum smooth muscles isolated from 7-week old GGPPS^SMKO and CTR mice. β-actin was employed as a loading control (n=5). *E*, the body weights of GGPPS^SMKO mice (n=6-17) and CTR mice. *F*, survival curve of GGPPS^SMKO and CTR mice (n=20). *G-J*, the forces of mesentery evoked by 124 mM KCl, 10 μM norepinephrine (NE) and 0.1 μM U46619 from 7-week old mice. n=5 for each group. All data are presented as mean ± s.e.m. of biologically independent samples with Student's unpaired t test. *, p<0.05; **, p<0.01; ***, p<0.001. *A.U.*, arbitrary units.
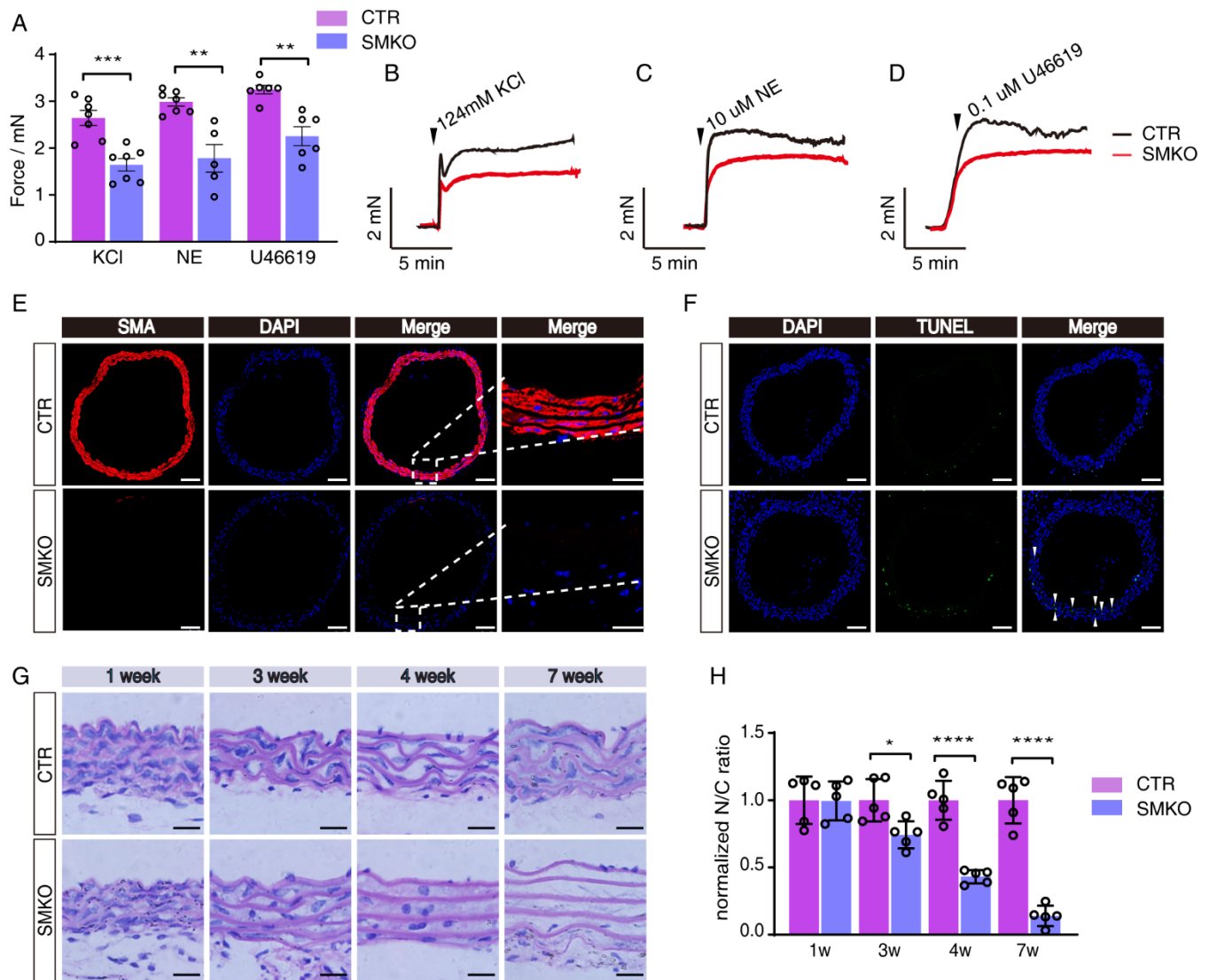
Figure 3. GGPPS deletion significantly impaired neonatal aorta smooth muscle by GGPP depletion. *A-D*, the forces of mesentery evoked by 124 mM KCl, 10 μM norepinephrine (NE) and 0.1 μM U46619 from 4-week old mice. n=5 for each group. *E*, staining smooth muscle cells with anti-SMA antibody and staining nuclei with DAPI dye. *Scale bars* are 25 μm. The *scale bars* in magnification frame are 100 μm. *F*, TUNEL assay for the apoptotic smooth muscle cells from 3-week old mice. *Scale bar*=100 μm. n=3 for each group. White arrow represents apoptotic cells. *G*, HE staining of aorta from 1-week (n=4), 3-week (n=5), 4-week (n=5) and 7-week (n=6) old mice. *Scale bar*, 20 μm. *H*, quantitation of nucleo-cytoplasmic ratio from *G*. All data are presented as mean ± s.e.m. of biologically independent samples with Student's unpaired t test. *, p<0.05; **, p<0.01; ***, p<0.001.
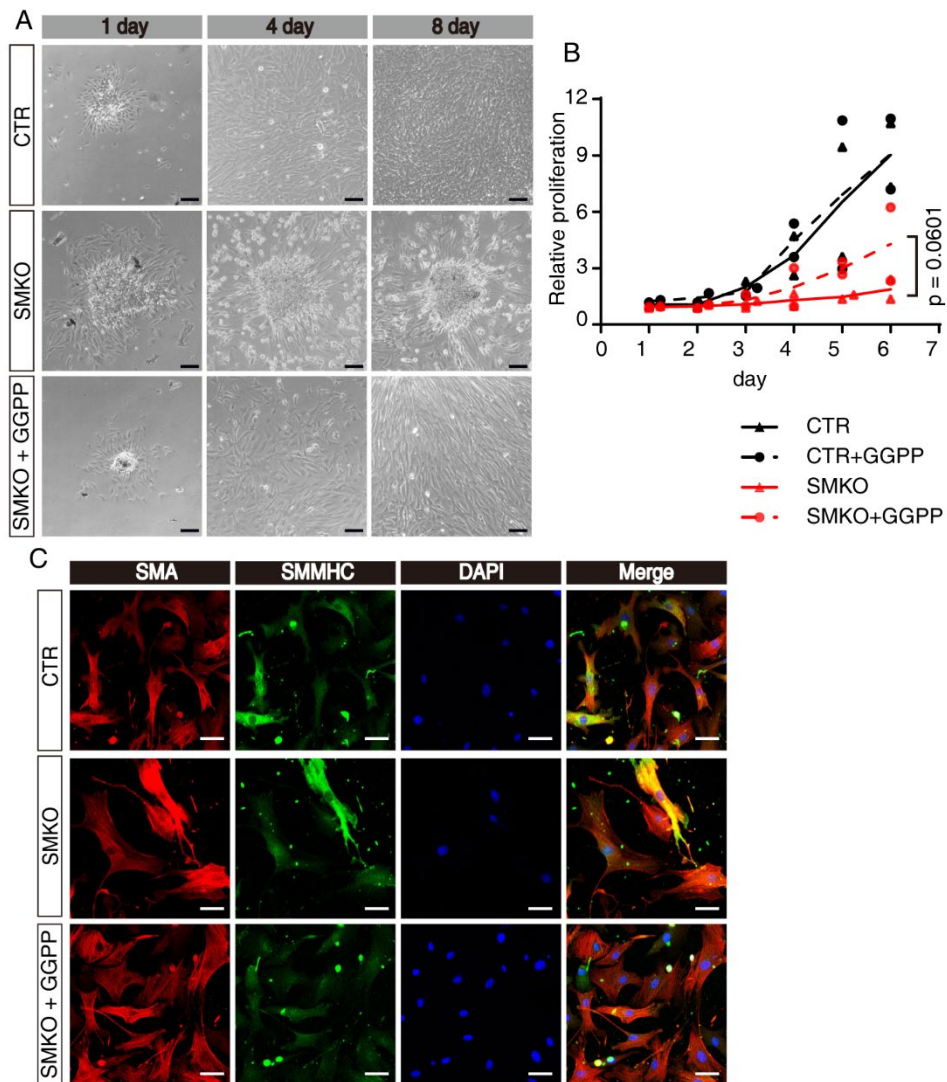
18

Figure 4. GGPPS deletion significantly impaired neonatal aorta smooth muscle by GGPP depletion. *A*, primary aorta smooth muscle cells isolated from GGPPS^{SMKO} and CTR mice at age of 14 days were incubated with or without 10 µM GGPP (n=5). *Scale bars* = 100 µm. *B*, cell proliferation of aorta smooth muscle cells from GGPPS^{SMKO} and CTR mice with or without 10 µM GGPP (n=3) were tested by cck-8. *C*, aorta smooth muscle cells were stained with DAPI and smooth muscle marker, SMA and SMMHC (n=3). *Scale bars* = 50 µm. Data of *B* are presented as mean ± s.e.m. of biologically independent samples with Two-way ANOVA followed with Bonferroni's test, ns, p>0.05; *, p<0.05; **, p<0.01; ***, p<0.001.
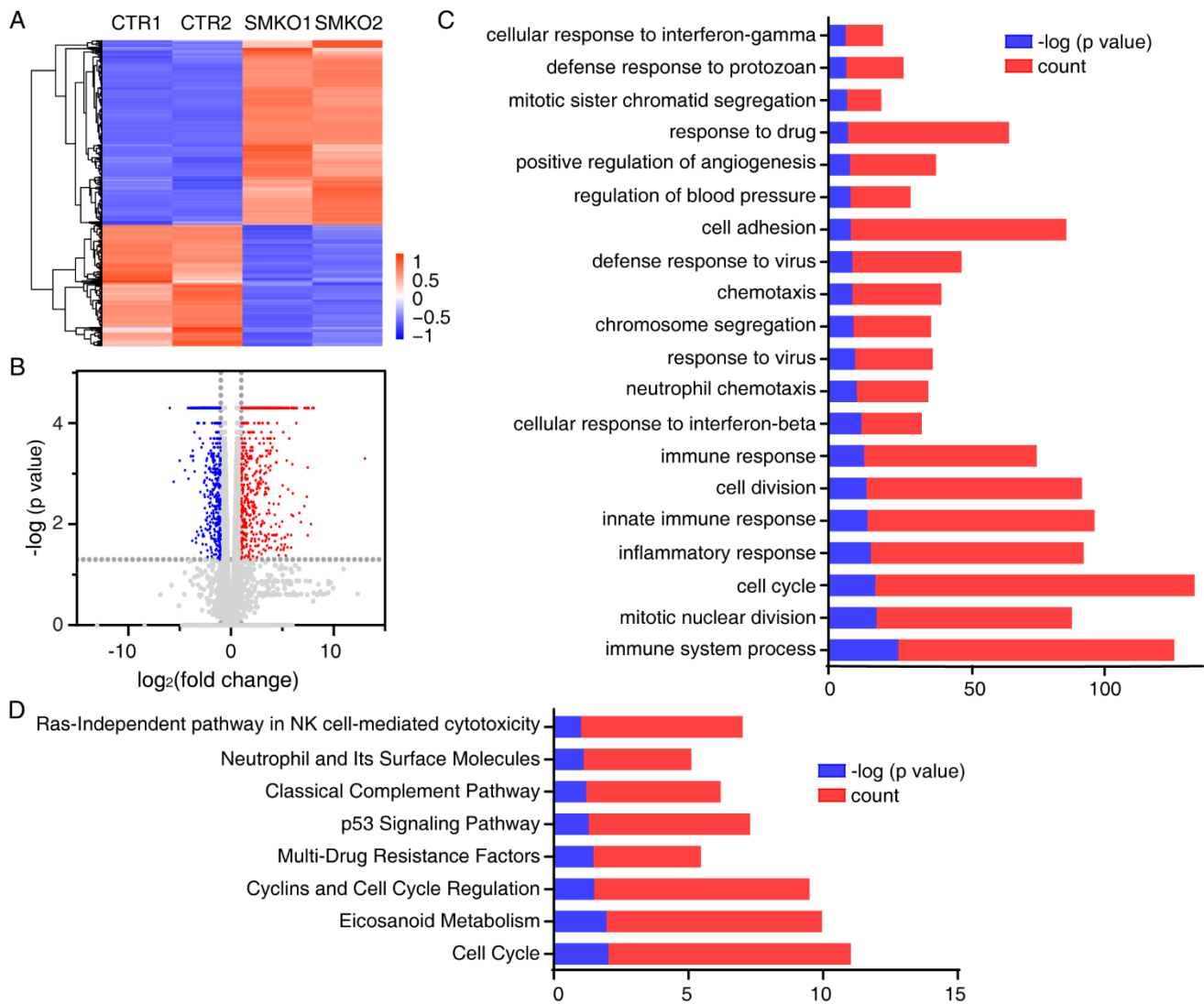
Figure 5. RNA-seq analysis of GGPPS-deficient aorta. *A*, heatmap of RNA-seq data from two independent pools from GGPPS[SMKO] and CTR individuals. *B*, volcano Plot of RNA-seq data from two independent pools from GGPPS[SMKO] and CTR individuals. *C*, functional categories analysis of gene transcripts by GOTERM. *D*, functional categories analysis of gene transcripts by BIOCARTA. The data was obtained from two independent pools. 3-week old mice were sacrificed and at least 10 aorta segments were pooled for each independent pool.
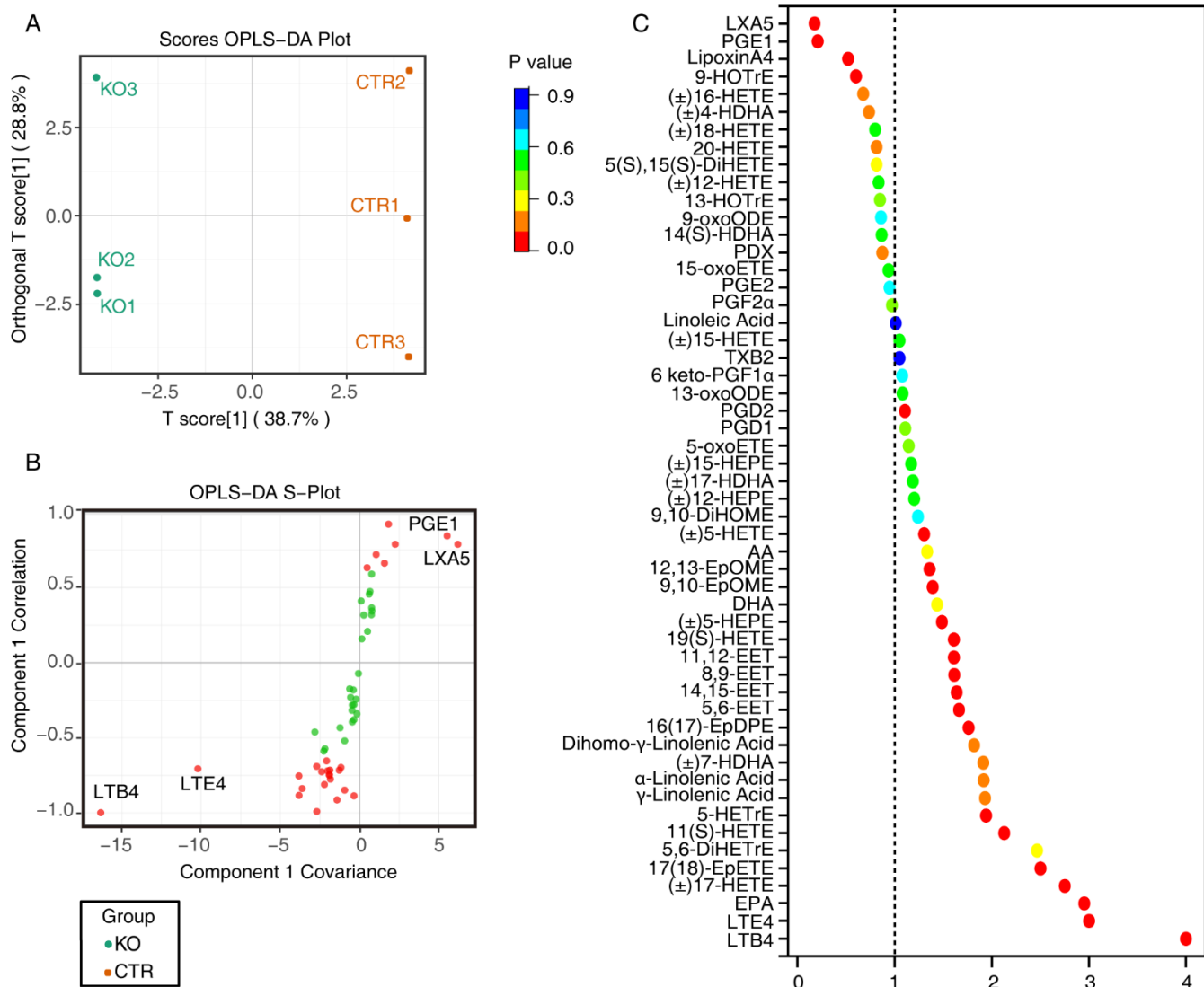
Figure 6. LC-MS analysis of eicosanoids metabolites in GGPPS deficiency aorta. *A*, orthogonal partial least-squares discriminant analysis (O-PLS-DA) scores plot illustrates separation between GGPPS[SMKO] and CTR individuals. *B*, the S-plot indicates the metabolites (highlighted in red) showing the highest absolute contribution to the association, with absolute values of covariance or correlation > 0.5 or < -0.5. *C*, measurement the concentration of eicosanoid metabolites related liposomes in GGPPS[SMKO] and CTR aorta by LC-MS. X-coordinate represents the fold change of SMKO to CTR. The data was obtained from three independent pools. Each independent pool was composed of 30 aortas.
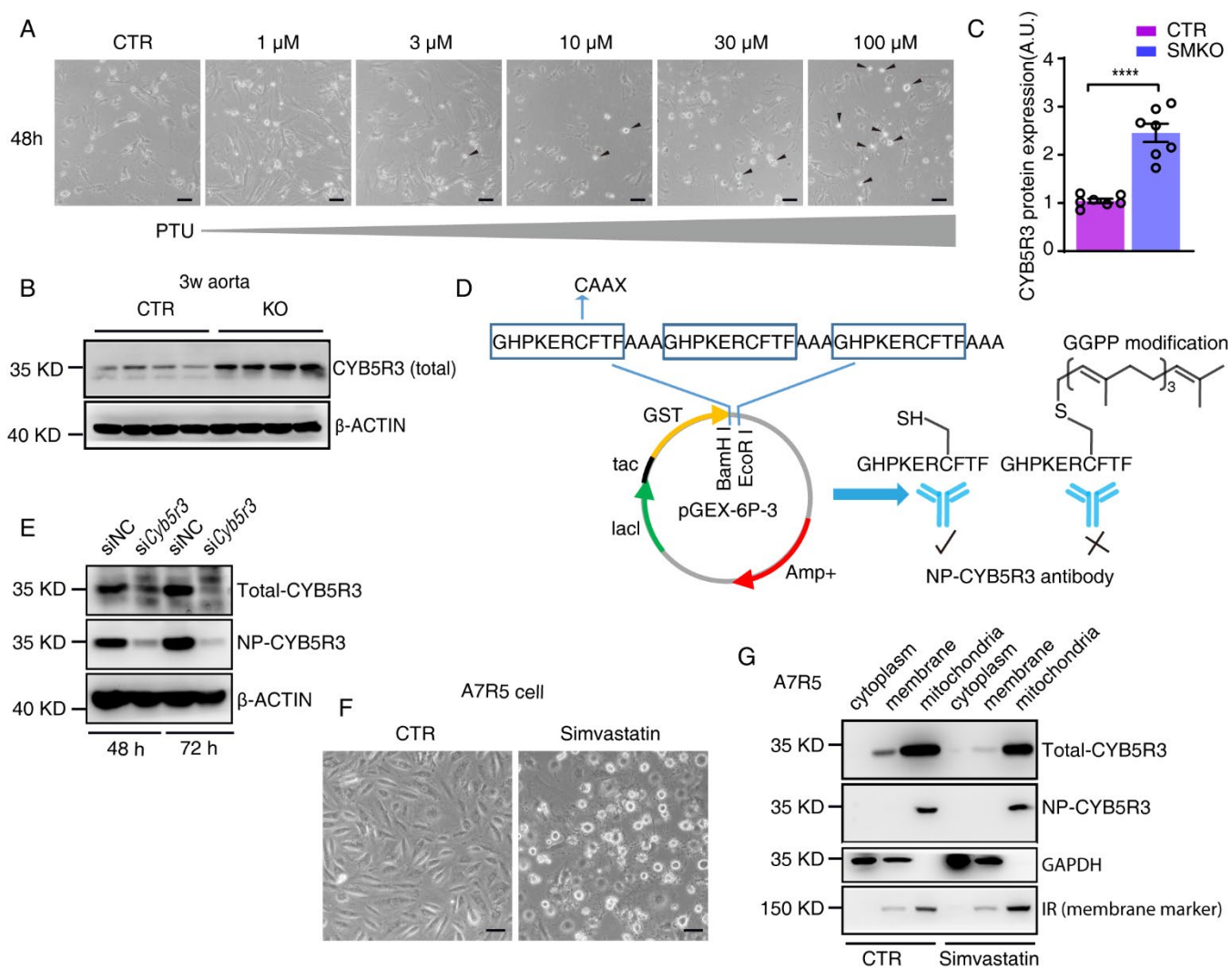
21

Figure 7. CYB5R3 prenylation of GGPP is required for anchorage at ER. *A*, inhibition of CYB5R3 activity by propylthiouracil (PTU) induced primary aorta smooth muscle cell death in a dose-dependent manner (n=3). *Scar bar*= 20 μm. Black arrow represents dead cells. *B-C*, protein expression of CYB5R3 in aorta was increased in 3-week old GGPPS^{SMKO} mice in contrast to CTR mice (n=7). *A.U.*, arbitrary units. All data are presented as mean ± s.e.m. of biologically independent samples with Student's unpaired t test, ****, p<0.0001. *D*, Strategy for making anti-NP-CYB5R3 antibody. A DNA fragment encoding three CAAX motifs was inserted into pGEX-6P-3 expressive vector to produce NP-CYB5R3 antibody in BALB/c mice. *E*, CYB5R3 protein was specifically recognized by NP-CYB5R3 antibody. The CYB5R3 expression in A7R5 cells was down-regulated by siRNA transfection. *F*, 10 μM simvastatin induced A7R5 cell death after 24 h *in vitro. Scar bar*= 20 μm. *G*, subcellular distribution of NP-CYB5R3 and total CYB5R3 in A7R5 cells. The fractions of cytoplasm, membrane and mitochondria were isolated from CTR and simvastatin-treated A7R5 cells. CYB5R3 protein was measured by Western blot with primary antibodies against to total CYB5R3 and NP-CYB5R3. GAPDH was used as cytoplasm marker, and IR (insulin receptor) was used as membrane marker.
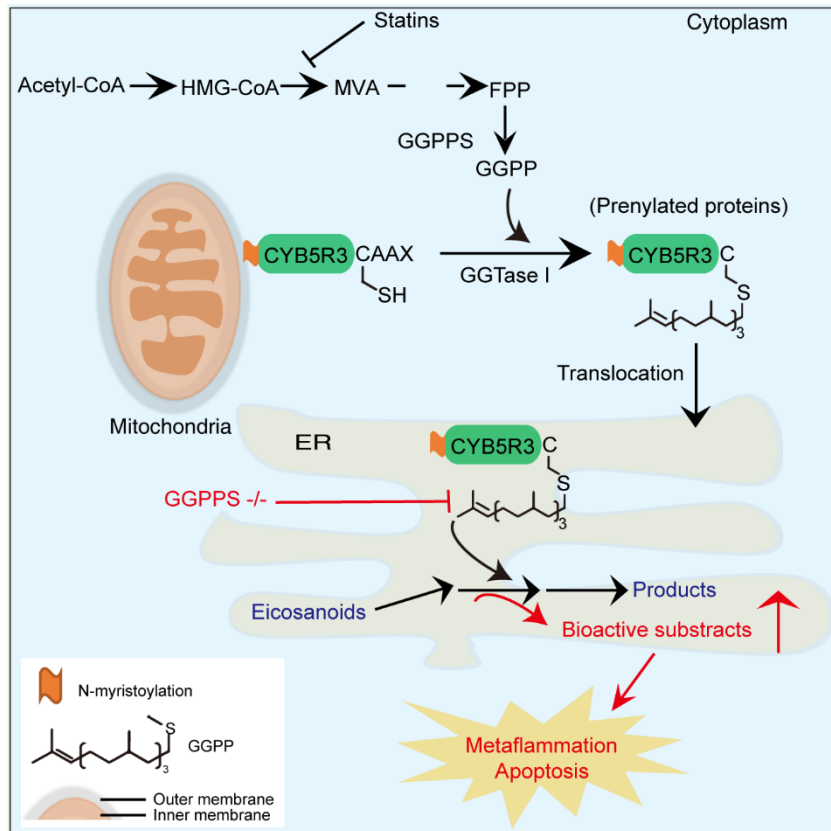
22

Figure 8. A model for the proposed role of MVA pathway in trigger of metaflammation. This model suggests that balance of eicosanoids metabolism is essentially required for neonatal vascular smooth muscle cells survival. Destroyed GGPP prenylation of CYB5R3 impairs eicosanoids metabolism homeostasis.

GGPP depletion initiates metaflammation through disequilibrating CYB5R3-dependent eicosanoid metabolism

Lisha Wei, Yan-Yan Zheng, Jie Sun, Pei Wang, Tao Tao, Yeqiong Li, Xin Chen, Yongjuan Sang, Danyang Chong, Wei Zhao, Yuwei Zhou, Ye Wang, Zhihui Jiang, Tiantian Qiu, Chao-Jun Li, Min-Sheng Zhu and Xuena Zhang

Access the most updated version of this article at doi: 10.1074/jbc.RA120.015020

Alerts:
- When this article is cited
- When a correction for this article is posted

Click here to choose from all of JBC's e-mail alerts